ACS OMEGA

Open Access

http://pubs.acs.org/journal/acsodf

Article

A Combined Approach for Rapid Dereplication of Herb−Drug Interaction Causative Agents in Botanical Extracts—A Molecular Networking Strategy To Identify Potential Pregnane X Receptor (PXR) Modulators in Yohimbe

Suresh Chandra V. A. R. Annam, William M. Neal, Pankaj Pandey, Bharathi Avula, Kumar Katragunta, Islam Husain, Shabana I. Khan, Igor Koturbash, Bill J. Gurley, Ikhlas A. Khan, and Amar G. Chittiboyina*

Cite This: *ACS Omega* 2024, 9, 51394−51407

Read Online

ACCESS | Metrics & More | Article Recommendations | Supporting Information

ABSTRACT: Despite promising preliminary biology, natural products isolation efforts may be confounded when the active compound is not isolated during bioassay-guided purification or classical pharmacognostic research investigations. A more rational isolation procedure connecting the polypharmacology of an herb to its individual constituents must be applied to better detect bioactive molecules before tedious analytical steps are considered. While *Pausinystalia johimbe* (yohimbe) has been traditionally used in herbal medicine as a general tonic, an aphrodisiac, a performance enhancer, and an integral part of various dietary supplements, the hydroethanolic extract of yohimbe was identified to possess at least 3−4-fold induction of the pregnane X receptor (PXR) at 30 μg/mL, a key nuclear receptor implicated in adverse interactions, *viz.*, herb−drug interactions (HDIs). For rapid dereplication of potential HDI agents within yohimbe, a novel MS/MS-based molecular networking analysis was integrated with *in vitro* data and *in silico* analysis of activity at PXR. Analysis of the molecular network of biologically active fractions resulted in the dereplication of three oxindole alkaloids, 14 indole alkaloids, and eight *N*-oxide alkaloids as the primary causative agents for PXR induction. The findings of this study indicate that this strategy could effectively guide the rapid dereplication of bioactive causative agents within complex botanical extracts. Additionally, it serves as a proof-of-concept for using integrated MS/MS-based molecular networking analysis to assess the safety profile of botanical supplements.

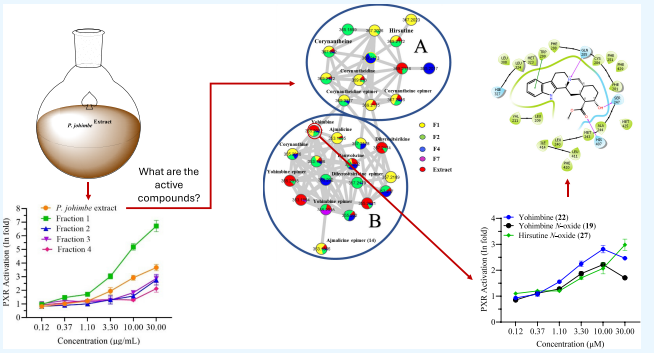

INTRODUCTION

Herbal medicines have been used for centuries to treat a wide range of human ailments.[1] The World Health Organization has established that botanical products are significant components of healthcare, with up to 80% of the population relying on herbal medicines and/or plant-derived drugs.[2] Considering the continued use of botanical natural products among the public, particularly concerning dietary supplements, herbs must be meticulously investigated for safety and efficacy, which presents a significant undertaking. In such investigations, the active compound(s) may not be isolated during subsequent bioassay-guided purification or classical phytochemical investigations, despite promising preliminary bioassay results of extracts. Moreover, herbs are typically complex in their composition, which complicates the identification, quantitation, and attribution of the activity of individual constituents.[3,4] Accordingly, most bioassay-guided fractionation efforts result in either repeated isolation of previously described molecules or the failure to identify the molecule(s) responsible for the observed bioactivity. Therefore, an isolation procedure that better detects bioactive molecules before extensive isolation steps are implemented should be rationally applied to medicinal herbs. Dereplication, or the use of chromatographic and spectroscopic analysis to recognize previously isolated substances present in an extract, is thus crucial to mitigate exhaustive scientific efforts when complex natural product mixtures are involved.

Pausinystalia johimbe (K. Schum.) Pierre ex Beille, commonly known as yohimbe, is an evergreen tree in the family Rubiaceae. Yohimbe is frequently touted as an herbal supplement for the treatment of sexual dysfunction in men on the basis of being administered traditionally in Africa as an aphrodisiac and for treating male sexual disorders.[5] In addition, yohimbe has been advertised as a local analgesic and performance enhancer,

Received: September 9, 2024
Revised: November 26, 2024
Accepted: November 29, 2024
Published: December 16, 2024

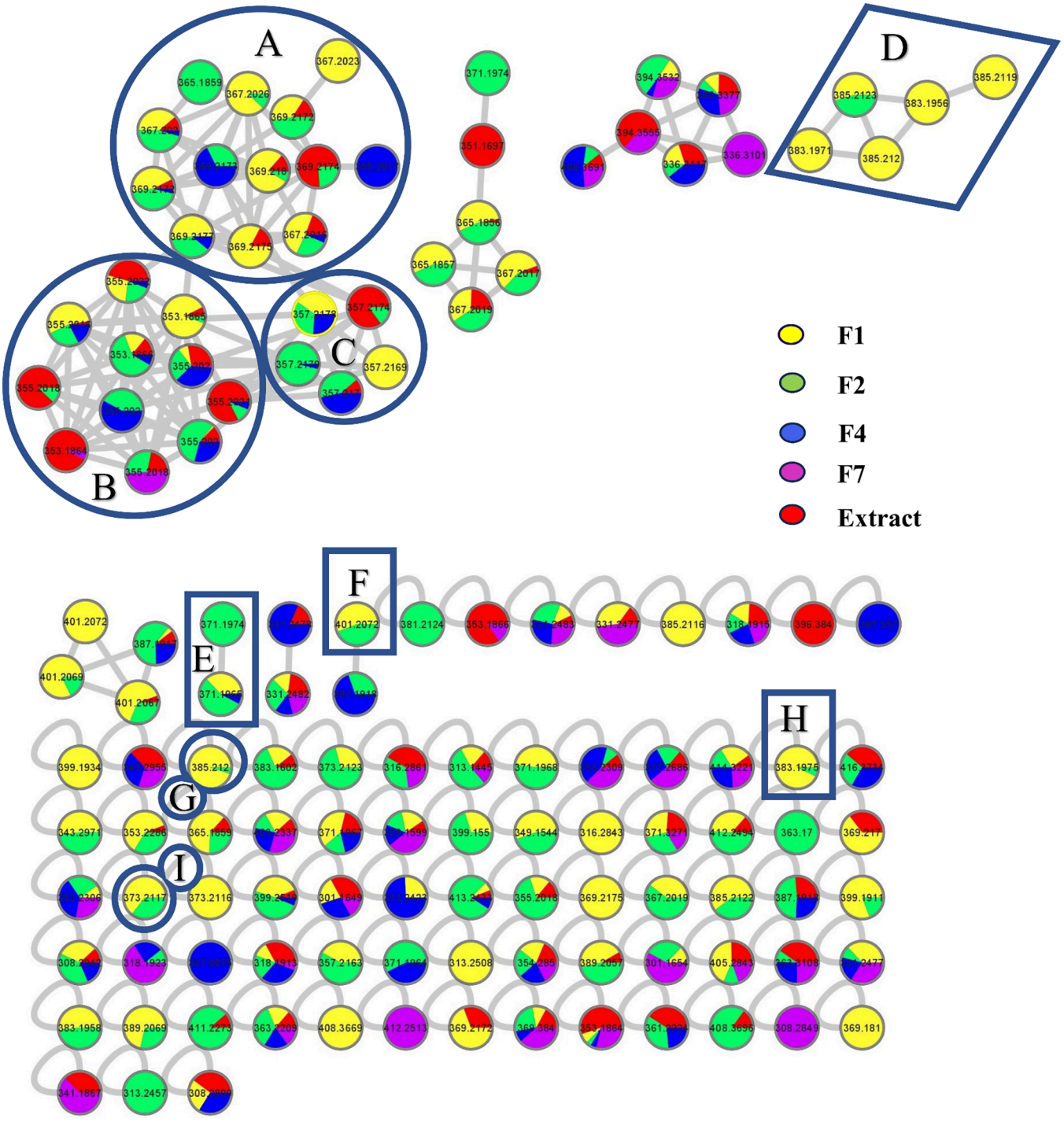

Figure 1. Networking of protonated molecules obtained from MS fragmentation of *P. johimbe* bark extract and fractions 1, 2, 4, and 7. Clusters A−B: indole alkaloids; Cluster C: unknown metabolites; Cluster D: oxindole alkaloids; Clusters E−I: *N*-oxide alkaloids.

increasing its popularity in over-the-counter supplements for athletes.[6−11] The primary bioactive components of yohimbe are indole alkaloids (≈3−6% of plant's composition), of which especially yohimbine and its related compounds possess a broad spectrum of biological activities.[12,13] Yohimbine, specifically, has been reported to be active at the α2-adrenergic receptor, as well as the serotonin and dopamine receptors, and has attracted significant scientific interest due to its polypharmacological effects.[13,14] However, yohimbine has also been associated with adverse effects, such as sympathomimetic toxicity.[13,15−18]

Additionally, there is evidence for the biotransformation of alkaloids, including indole alkaloids, regarding the oxidation of the *N*-4 substituent.[19,20] Complicating the structure−activity relationship of biotransformed alkaloids is the stereoselective production of a scalemic mixture of enantiomeric *N*-oxides, which has been shown to occur with a structurally diverse array of alkaloids.[19−21] Notably, a 2018 study on *P. johimbe* revealed the debatable existence of both enantiomeric *N*-oxide analogs of several alkaloids present in yohimbe.[22] It is postulated that the oxidation of alkaloids in plants is intended to improve the hydrophilicity of the compounds in order to aid in their active

https://doi.org/10.1021/acsomega.4c08293
ACS Omega 2024, 9, 51394−51407

cellular transport and storage.[23] However, the functionalization of the *N*-4 substituent is hypothesized to alter the *in vivo* pharmacological properties of the alkaloids compared to their parent tertiary amines.

Despite the continued interest in its aphrodisiac effects, there is a dearth of knowledge surrounding the effects of *P. johimbe* on human metabolism. Jabir et al. hypothesize yohimbe as an ideal ligand for several human G-protein coupled receptors (GPCRs), particularly in the interest of anticancer activity.[13] However, *Hypericum perforatum* L. (St. John's wort), another medicinal herb with activity at serotonin and dopamine GPCRs, has been shown to contain compounds with significant pregnane X receptor (PXR) inductive activity.[24,25] PXR (hPXR, *NR1I2*) is a nuclear receptor (NR), a family of ligand-regulated transcription factors that directly influence transcription of genes that control cell proliferation, development, metabolism, and reproduction.[26,27] Additionally, some experimental evidence suggests that yohimbine-containing products can affect the hepatic expression of a number of PXR downstream targets, e.g., Cd36 – a fatty acid uptake transporter.[18] PXR is poised as a NR target for complex natural products, since, unlike the majority of NRs, PXR exhibits a larger and more flexible ligand binding domain (LBD), allowing for a greater structural diversity of ligands to bind.[27−29] Notably, PXR is associated with major cytochrome P450 (CYP450) genes which encode essential enzymes that are responsible for the metabolism of various xenobiotics.[30,31] Botanical modulation of CYP450 activity that leads to marked alteration in the pharmacokinetics of coadministered pharmaceuticals is considered an herb-drug interaction (HDI), which may result in deleterious side effects. It was subsequently hypothesized that HDIs involving yohimbe could result from toxicity associated with compounds in *P. johimbe* that induce PXR activity.

To support this hypothesis, this study integrated mass spectrometry (MS) with Global Natural Products Social Molecular Networking (GNPS) methodology in combination with biological activity. The recent implementation of GNPS has revolutionized natural product discovery and characterization by clustering compounds based on similar mass spectral features, thereby enabling systematic comparison and rapid identification of compounds by grouping fragments into clusters based on their tandem mass spectrometry (MS/MS) data.[32]

The primary objective of this study was to rapidly dereplicate the causative agents in yohimbe responsible for PXR activation without performing intensive pharmacognosy steps. GNPS was coupled with liquid chromatography (LC) to ascertain the alkaloids present in biologically active (i.e., PXR-active) yohimbe samples. Furthermore, the inductive activity of fractions from yohimbe extract and of individual alkaloids identified from these fractions was validated *in vitro* for PXR modulation. *In silico* molecular docking provided insights into the variations in activities observed for the yohimbe alkaloids. Altogether, this holistic approach aimed to provide a proof-of-concept for employing an integrated MS/MS-based molecular networking analysis as a tool to determine the safety of botanical supplements.

RESULTS AND DISCUSSION

GNPS Network of Alkaloids from *P. johimbe*. To create a GNPS network of alkaloids from *P. johimbe*, the ethanolic extract and associated fractions of *P. johimbe* bark were profiled by UHPLC-QToF-MS (positive ion mode). The resultant data was subjected to a feature-based molecular networking workflow using MZmine2 (https://mzmine.github.io), hosted through the online GNPS server (http://gnps.ucsd.edu). The generated molecular networks were visualized in Cytoscape (v3.7.1). Following metabolite organization based on MS/MS spectral similarity, the data were compared to the GNPS molecular networking library. A total of 134 precursor protonated molecules were generated and illustrated as nodes in the molecular map, which included 8 clusters (number of nodes (n) ≥ 2) and 77 single nodes. The results revealed 6 distinct alkaloid clusters ($n \geq 4$) as shown in Figure 1.

GNPS efficiently separated indole alkaloids (clusters A-B) from oxindole alkaloids (cluster D). Nodes belonging to precursor protonated molecules with identical *m*/*z* values were annotated as identical structures. This was interpreted to result from a molecular family consisting of a group of stereoisomers that formed clusters A, B, and C (Figure 2). Such stereoisomers often exhibit very similar MS/MS spectra.

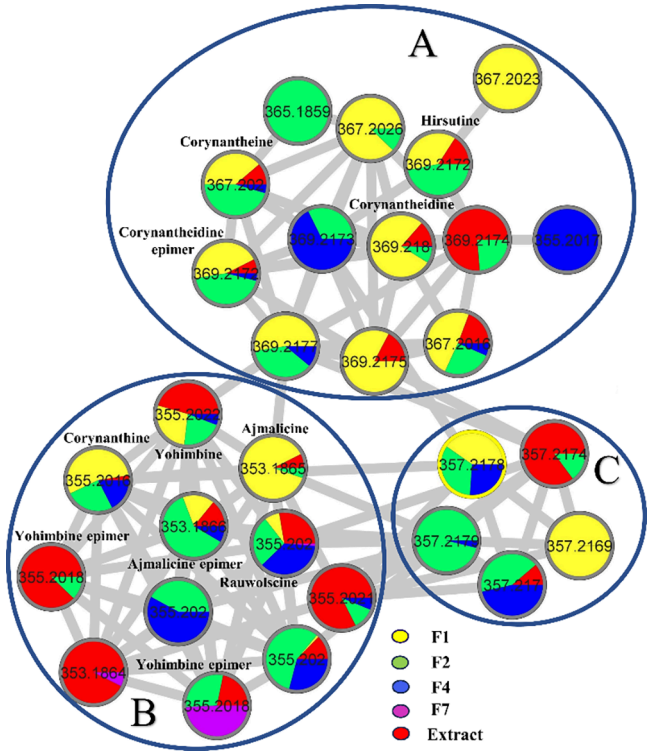

Figure 2. *Enlarged view of indole alkaloid clusters obtained from GNPS.* Cluster A: corynantheine-type alkaloids; Cluster B: yohimbine- and heteroyohimbine-type alkaloids; Cluster C: unknown metabolites.

Cluster A (Figure 2 and Table 1) was primarily composed of epimeric indole alkaloids with *m*/*z* 367 and 369. Nodes showed *m*/*z* 369.2169 (RT-22.14 min), 369.2161 (RT-23.23 min), and 369.2158 (RT-27.71 min) (Figure 2 and Table 1), which corresponded to the molecular formula $C_{22}H_{29}N_2O_3$ $[M + H]^+$ and were tentatively identified as corynantheine-type alkaloids.[33]

Key fragments (protonated) of compounds from Cluster A (Figure 2) were detected at *m*/*z* 337.1900, 253.1644, 238.1404, 226.1415, and 144.0807. Ring cleavage at C-2,3 and *N*-4, C-5 resulted in the formation of an indole derivative with *m*/*z* 144.0807 $[C_{10}H_{10}N]^+$. Similarly, ring cleavage at C-2,3 and C-5,6 resulted in the formation of a protonated molecule with *m*/*z* 226.1415 $[C_{12}H_{20}NO_3]^+$. Loss of C_9H_9N from the protonated

https://doi.org/10.1021/acsomega.4c08293
ACS Omega 2024, 9, 51394−51407

Table 1. Tentative Alkaloid Identification in Extract Fractions (F1, F2, F4, and F7) by UHPLC-QToF-MS/MS in Positive Ion Mode

S. No.	RT (min)	Mass $[M + H]^+$ (Da) Detected	Calculated	Error (ppm)	Molecular formula	MS/MS	Tentative ID
1	11.63	355.2020	355.2016	1.12	$C_{21}H_{26}N_2O_3$	224.1266, 212.1255, 194.1150, 144.0804	Corynanthine (**21**)
2	13.01	355.2013	355.2016	−0.84	$C_{21}H_{26}N_2O_3$	224.1296, 212.1282,194.1157, 144.0816	Yohimbine epimer (**24**)
3	13.57	355.2015	355.2016	−0.28	$C_{21}H_{26}N_2O_3$	224.1294, 212.1262, 194.1134, 144.0805	Yohimbine epimer (**25**)
4	13.89	355.2008	355.2016	−2.25	$C_{21}H_{26}N_2O_3$	224.1263, 212.1265, 194.1148, 144.0801	Yohimbine (**22**)
5	14.25	355.2010	355.2016	−1.68	$C_{21}H_{26}N_2O_3$	224.1287, 212.1287, 194.1127, 144.0807	Rauwolscine (**23**)
6	14.37	357.2166	357.2173	−1.95	$C_{21}H_{28}N_2O_3$	251.1532, 226.1427, 214.1436, 144.0813	Dihydrositsirikine (**16**)
7	15.01	357.2173	357.2173	0.00	$C_{21}H_{28}N_2O_3$	251.1525, 226.1430, 214.1406, 144.0811	Dihydrositsirikine epimer (**17**)
8	15.48	373.2118	373.2122	1.03	$C_{21}H_{28}N_2O_4$	355.2009, 341.1868, 325.1912, 251.1539, 225.1386, 197.1062, 144.0808	Dihydrositsirikine *N*-oxide (**18**)
9	16.02	383.1960	383.1965	1.39	$C_{22}H_{26}N_2O_4$	351.1705, 319.1458, 265.1305, 239.1182, 224.1303, 187.0861, 160.0754, 132.0802	Corynoxeine (**11**)
10	16.59	371.1962	371.1965	−0.81	$C_{21}H_{26}N_2O_4$	353.1850, 335.1751, 321.1605, 223.1216, 197.1047	Yohimbine *N*-oxide (**19**)
11	17.41	385.2117	385.2122	1.29	$C_{22}H_{28}N_2O_4$	353.1857, 267.1477, 241.1333, 226.1426, 194.1148, 187.0861, 160.0755	Isorhynchophylline (**9**)
12	18.03	371.1960	371.1965	1.34	$C_{21}H_{26}N_2O_4$	353.1859, 335.1724, 321.1579, 223.1206, 197.1062, 156.0783	Yohimbine *N*-oxide epimer (**20**)
13	18.14	399.1914	399.1914	0.00	$C_{22}H_{26}N_2O_5$	381.1796, 265.1310, 236.1274, 160.0742, 132.0795	Corynantheine pseudoindoxyl *N*-oxide (**13**) or its isomer
14	18.72	353.1865	353.1860	−1.41	$C_{21}H_{24}N_2O_3$	222.1147, 210.1115, 190.0863, 178.0858, 144.0811, 117.0699	Ajmalicine (**14**)
15	20.05	401.2064	401.2071	1.74	$C_{22}H_{28}N_2O_5$	383.1938, 369.1789, 267.1514, 238.1430, 224.1273, 213.1053, 160.0754	Dihydrocorynantheine pseudoindoxyl *N*-oxide (**12**) or its isomer
16	20.78	353.1861	353.1860	0.28	$C_{21}H_{24}N_2O_3$	222.1165, 210.1127, 190.0863, 178.0870, 144.0810, 117.0698	Ajmalicine epimer (**15**)
17	21.88	367.2015	367.2016	0.27	$C_{22}H_{26}N_2O_3$	335.1762, 251.1525, 236.1262, 224.1259, 144.0802	Corynantheine (**4**)
18	22.14	369.2169	369.2173	−1.08	$C_{22}H_{28}N_2O_3$	337.1900, 253.1644, 238.1404, 226.1415, 144.0807	Corynantheidine (**1**)
19	22.42	385.2124	385.2122	−0.51	$C_{22}H_{28}N_2O_4$	267.1514, 241.1326, 226.1427, 160.0763	Corynoxine (**10**)
20	22.92	385.2130	385.2122	2.07	$C_{22}H_{28}N_2O_4$	367.2012, 353.1852, 251.1542, 225.1378, 197.1063, 184.0988, 156.0803, 144.0804	Corynantheidine *N*-oxide epimer (**7**)
21	23.23	369.2161	369.2173	3.25	$C_{22}H_{28}N_2O_3$	337.1900, 253.1644, 238.1404, 226.1415, 144.0800	Corynantheidine epimer (**2**)
22	25.30	367.2014	367.2016	−0.54	$C_{22}H_{26}N_2O_3$	335.1714, 251.1528, 236.1251, 224.1258, 144.0793	Geissoschizine methyl ether or corynantheine epimer (**5**)
23	25.64	383.1960	383.1965	−1.30	$C_{22}H_{26}N_2O_4$	365.1842, 351.1708, 249.1370, 223.1212, 197.1060, 184.0985, 156.0791, 144.0795	Corynantheine *N*-oxide (**8**)
24	26.76	385.2127	385.2122	1.29	$C_{22}H_{28}N_2O_4$	367.2032, 353.1860, 251.1548, 225.1390, 197.1065, 184.0999, 156.0817, 144.0820, 132.0806	Corynantheidine *N*-oxide (**6**)
25	27.71	369.2158	369.2173	−3.52	$C_{22}H_{28}N_2O_3$	253.1684, 238.1442, 226.1479, 144.0829	Hirsutine (**3**)

molecule resulted in m/z 238.1404 $[C_{13}H_{20}NO_3]^+$. The presence of a product ion at m/z 253.1644 indicated that cleavage of the methoxy acrylate moiety could occur via McLafferty rearrangement (Figure 4A). Based on literature data and mass fragmentation, these epimeric compounds (Figure 3 and Figures S1−S3) were tentatively identified as corynantheidine (**1**), corynantheidine epimer (**2**), and hirsutine (**3**).[33]

Additionally, the identity of the latter compound, **3**, was further corroborated by a comparison with the retention time and fragmentation pattern of the reference standard of hirsutine (**3**) (Figure S26). The proposed fragmentation pathway is shown in Figure 4A.

Additional nodes in Cluster A (Figure 2) yielded a protonated molecule at m/z 367.2015 $[M + H]^+$ (RT-21.88 min) and m/z 367.2014 (RT-25.30 min). The accurate mass measurement suggested that the elemental composition was $C_{22}H_{27}N_2O_3$ $[M + H]^+$, consisting of two hydrogen atoms less than corynantheidine. In the MS/MS spectra, characteristic fragment protonated molecules at m/z 251.1525 $[C_{17}H_{19}N_2]^+$, 236.1262 $[C_{13}H_{18}NO_3]^+$, and 224.1259 $[C_{12}H_{18}NO_3]^+$ were observed, suggesting the ethyl group at C-20 in corynantheidine had been substituted with an ethylene group in **4** and **5** (Figure 3). However, the retention times of these compounds (Figures S4−S5) did not correspond to the known retention time of hirsuteine (**26**) (Figure S27). Thus, the structures of **4** and **5** were tentatively identified as corynantheine and geissoschizine methyl ether or corynantheine epimer.[34]

Compounds **6** and **7** from Cluster G (Figure 1) possessed protonated molecules at m/z 385.2127 $[M + H]^+$ (RT-26.76 min) and 385.2130 $[M + H]^+$ (RT-22.92 min)-16 Da more than that of hirsutine (**3**). The accurate mass of these protonated molecules suggested that their elemental composition was $C_{22}H_{28}N_2O_4$. Key fragments detected were at m/z 367.2032, 353.1860, 251.1548, 225.1390, 197.1065, 184.0999, 156.0817, 144.0820, and 132.0806. An m/z of 353.1860 $[C_{21}H_{25}N_2O_3]^+$ corresponded to a loss of methanol from the pronated molecule. The ion at m/z 367.2032, resulting from dehydration $[M+H-H_2O]^+$, underwent sequential fragmentation, producing two distinct product ions: m/z 251.1548 $[C_{17}H_{19}N_2]^+$ through McLafferty rearrangement and m/z 184.0999 through *retro*-Diels−Alder cleavage (Figure 4B). The MS/MS results suggested that compound **6** is structurally similar to hirsutine except for an additional oxygen atom that was attached to *N*-4 in **6**. The retention time values of compounds **6** and **7** did not

https://doi.org/10.1021/acsomega.4c08293
ACS Omega 2024, 9, 51394−51407

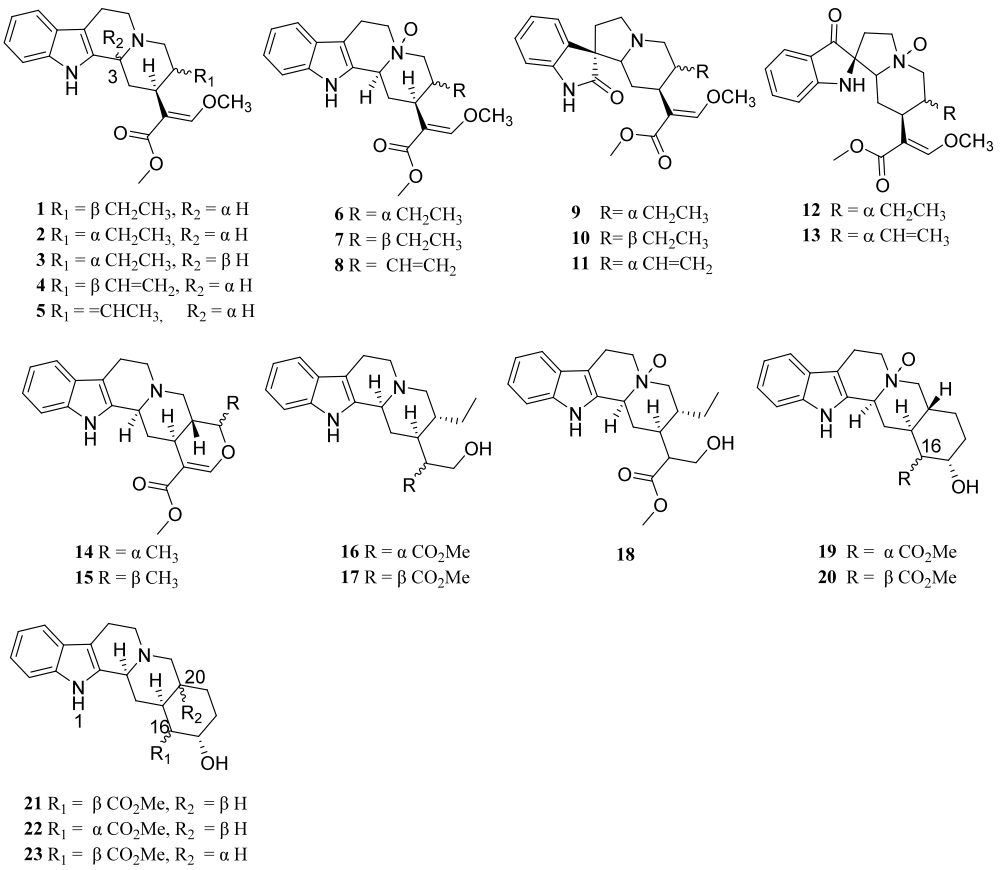

Figure 3. Structures of compounds (**1**−**23**) from *P. johimbe*.

correspond to the retention time of the hirsutine *N*-oxide reference standard (Figures S28−S29).[35] The structures of compounds **6** and **7** have been tentatively assigned as corynantheidine *N*-oxide (Figure S6) and its epimer (Figure S7), and the proposed fragmentation pathway for compound **6** is depicted in Figure 4B.

Compound **8** in cluster H (Figure 1) generated a protonated molecule with *m*/*z* 383.1960 $[M+H]^+$ corresponding to the molecular formula $C_{22}H_{26}N_2O_4$. Its MS/MS spectra were similar to those of compound **6**. Key protonated molecules at *m*/*z* 365.1842 $[M+H-H_2O]^+$, 351.1708 $[M+H-CH_3OH]^+$, and 249.1370 $[M+H-C_5H_9O_4]^+$ were observed, suggesting that the ethyl group in compound **6** had been substituted with a vinyl group in compound **8** (Figure S8). Compound **8**, which was observed at 25.64 min, did not correspond to the retention time of the hirsuteine *N*-oxide reference standard (Figures S30−S31).[35] Thus, the structure of compound **8** was tentatively identified as corynantheine *N*-oxide (or its epimer).

In cluster D (Figure 1), isomeric compounds at *m*/*z* 385.2117 (RT-17.41 min) and 385.2124 (RT-22.42 min) were tentatively identified as isorhynchophylline (**9**, Figure S9) and corynoxine (**10**, Figure S10) or its isomers through the GNPS library and their specific MS/MS data. Key protonated molecules were found at *m*/*z* 353.1857, 267.1477, 241.1333, 226.1426, 187.0861, 160.0755 (Table 1). The protonated molecule at *m*/*z* 353.1857 $[M+H-CH_3OH]^+$ possessed the same fragmentation pattern as hirsutine (**3**); however, the presence of a carbonyl group adjacent to the nitrogen in the indole group indicated an oxindole alkaloid rather than an indole alkaloid. The peak at 267.1477 $[M+H-128]^+$ resulted from the loss of a methoxy acrylate moiety (Figure 5A). Indeed, cleavage of the ring at C-2,3 and *N*-4, C-5 positions yielded an oxindole fragment detected at *m*/*z* 160.0755 $[C_{10}H_{10}NO^+]$. The proposed fragmentation pathway for compound **10** is shown in Figure 5A and Figure S10.

A compound with *m*/*z* 383.1960 was tentatively identified as corynoxeine (**11**) or its diastereomer, and its MS/MS showed characteristic fragment ions at *m*/*z* 351.1705 $[M+H-32]^+$, 265.1305 $[M+H-128]^+$, and 160.0754 $[M+H-225]^+$ (Figure S11).

Compound **12** generated a protonated molecule with *m*/*z* 401.2064 as found in cluster F (Figure 1), corresponding to the molecular formula $C_{22}H_{28}N_2O_5$. The key fragment protonated molecules appeared at *m*/*z* 383.1938, 369.1789, 267.1514, 238.1430, 224.1273, 213.1053, 192.0991, 187.0875, and 160.0754. MS/MS results suggested that compound **12** is structurally similar to corynoxiene or its epimer, except for an additional oxygen atom that was attached to *N*-4. Thus, the structure of **12** was tentatively identified as dihydrocorynantheine pseudoindoxyl *N*-oxide (**12** or its epimer) (Figures S12).

Compound **13** fragmented into a protonated molecule with *m*/*z* 399.1914 $[M + H]^+$ in cluster D (Figure 1), corresponding to the molecular formula of $C_{22}H_{26}N_2O_5$. Its MS/MS spectra are similar to those of compound **6**. Notable fragment protonated molecules at *m*/*z* 381.1796 $[M+H-H_2O]^+$, 265.1335 $[M+H-C_5H_8O_3]^+$ and 236.1274 $[M+H-C_9H_7NO]$ were observed, suggesting that the ethyl group in compound **12** had been substituted with a vinyl group in compound **13** (Table 1 and Figure S13). Thus, the structure of **13** was tentatively identified as corynantheine pseudoindoxyl *N*-oxide (**13**) or its epimer.

At 18.72 and 20.78 min, MS/MS-spectra-associated chromatographic peaks were observed for a precursor ion with *m*/*z*

https://doi.org/10.1021/acsomega.4c08293
ACS Omega 2024, 9, 51394−51407

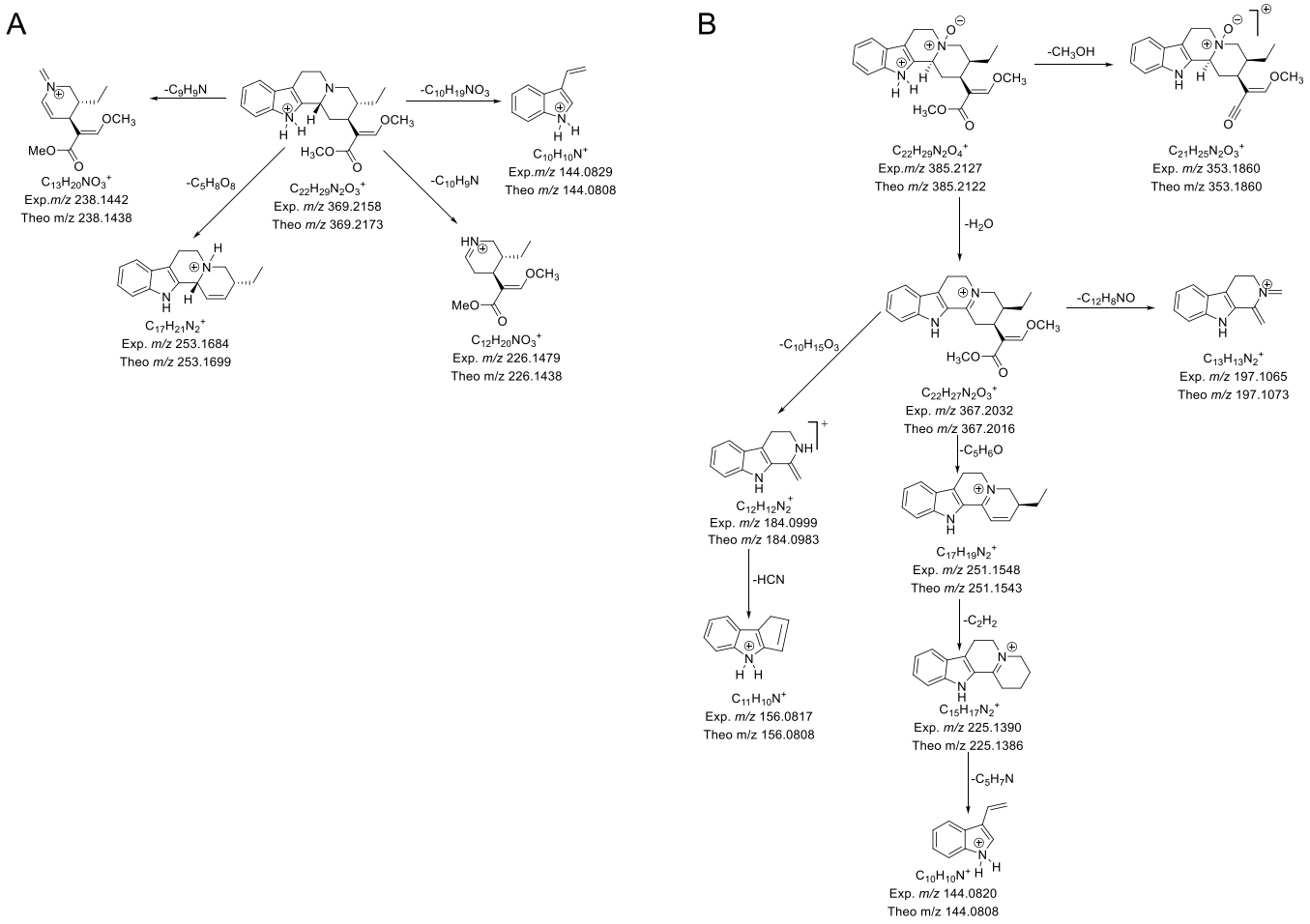

Figure 4. Proposed fragmentation patterns of (**A**) hirsutine (**3**) and (**B**) corynantheidine *N*-oxide (**6**).

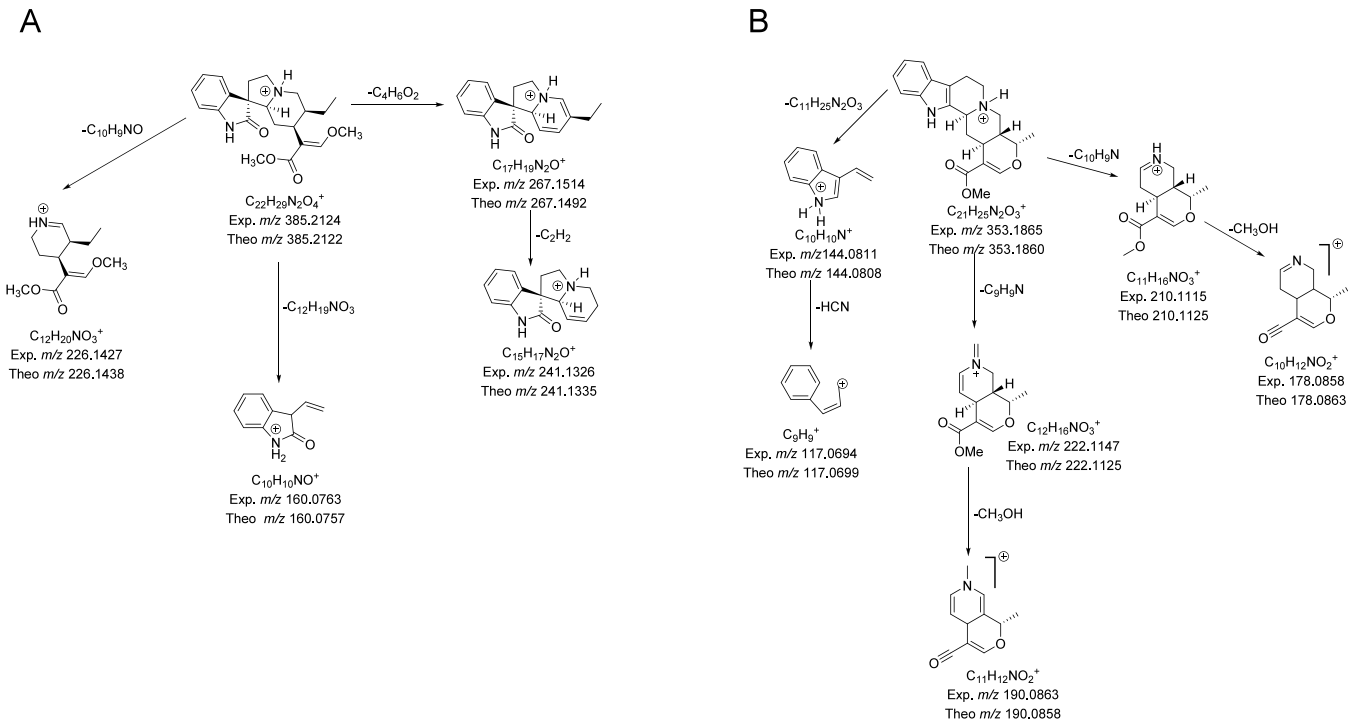

Figure 5. Proposed fragmentation patterns of (**A**) corynoxine (**10**) and (**B**) ajmalicine (**14**).

https://doi.org/10.1021/acsomega.4c08293
ACS Omega 2024, 9, 51394−51407

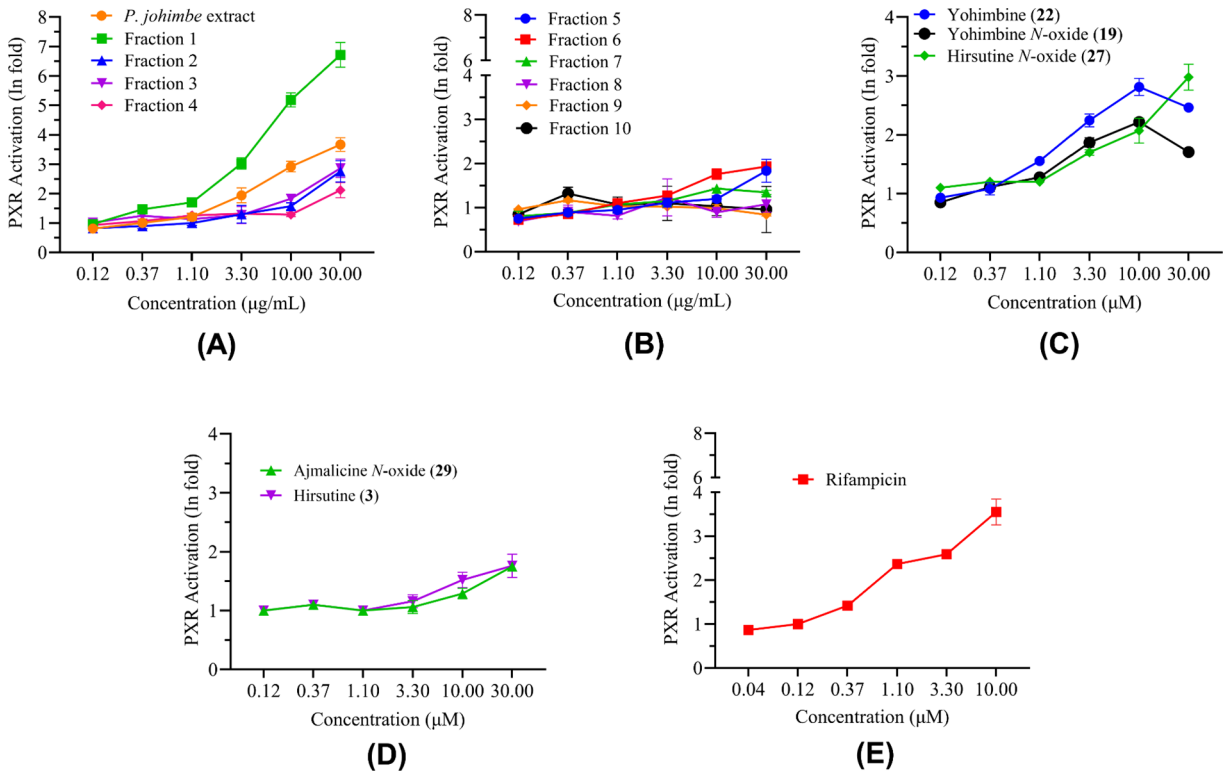

Figure 6. Effect of *P. johimbe* extract and its major alkaloids on the activity of hPXR in HepG2 cells. (A) Extract and fractions 1−4 of *P. johimbe*, (B) fractions 5−10 of *P. johimbe*, (C) pure alkaloids, (D) inactive compounds, (E) positive control. The hepatic (HepG2) cells in the logarithmic phase were transfected with the PXR plasmid and treated with the indicated concentrations of test samples for 24 h. Following incubation, PXR activity was measured in triplicate.

353.1865 $[M + H]^+$. Based on the molecular features, including fragment ions, these compounds were tentatively identified as ajmalicine (**14**) and its epimer (**15**). Detailed information about MS/MS fragments for compounds **14** and **15** (Cluster B) is arranged in Table 1.[35] MS/MS analysis of these compounds revealed significant protonated molecules at m/z 222.1165, 210.1117, 190.0863, 178.0870, 144.0810, 117.0698 (Table 1 and Figures 5B, S14−S15). Compound **14** was identified and characterized by further comparison to the authentic standard of ajmalicine (Figure S34). The proposed fragmentation pathway is shown in Figure 5B. The mass spectral data of the reference standard of ajmalicine *N*-oxide (**29**) was compared with mass spectral data of the extract. While the retention time of compound **29** matched with the retention time of **1** (RT-22.14), mass values indicated that **29** was not present in the yohimbe extract (Figures S35−S36). Similarly, compounds **16** and **17** possessed a m/z 357 (Figures S16−S17). Compounds **16** and **17** were thus tentatively identified as dihydrositsirikine and its epimer (Table 1).

Compound **18** generated a protonated molecule with m/z 373.2118 $[M + H]^+$ in cluster I (Figure 1) consistent with the molecular formula $C_{21}H_{28}N_2O_4$. Since the MS/MS results suggested that compound **18** is structurally similar to dihydrositsirikine except for an additional oxygen atom attached to *N*-4, the structure of **18** was tentatively identified as dihydrositsirikine *N*-oxide (Figure S18).

In cluster B (Figure 2), additional nodes with m/z 355 were identified as corynanthine (**21**), yohimbine (**22**) and its epimers (**24** and **25**), and rauwolscine (**23**), as shown in Figures S21−S25. These compounds were further verified according to their chemical standards (Figure S32). In cluster D (Figure 1), nodes revealed protonated molecules $[M + H]^+$ at m/z 371.1962 (RT-16.59 min) and 371.1960 (RT-18.03 min). Accurate mass measurement suggested that their elemental composition was $C_{21}H_{26}N_2O_4$, one oxygen atom more than yohimbine. Additionally, the MS/MS results suggested that compounds **19** and **20** are structurally similar to yohimbine, apart from an additional oxygen atom bound to *N*-4 in both **19** and **20**. Notably, the retention time of compound **19** (RT-16.59 min) corresponded to the retention time of the yohimbine *N*-oxide reference standard (Figure S33).[35] From these results, the structures of compounds **19** and **20** have been assigned as yohimbine *N*-oxide and its epimer, respectively, and the associated proposed fragmentation pathways are shown in Figures S19 and S20.

***In Vitro* PXR Activation by Yohimbe Alkaloids.** As identified through the previous steps, *P. johimbe* contains a diverse range of phytochemicals, including not only corynantheine-, yohimbine-, and heteroyohimbine-type alkaloids but also oxindole alkaloids. Considering the continued use of *P. johimbe* in the herbal supplement industry, the prevalence of HDIs with botanical natural products, and the lack of scientific evidence to support the safety of yohimbe, it was deemed prudent to establish the activities of the identified yohimbe alkaloids at PXR.

This study investigated the PXR activation potency of fractions prepared from *P. johimbe* extract and its pure alkaloids (Figure 6).

The *P. johimbe* extract exhibited a dose-dependent PXR activation, with a maximal 3.66-fold increase at 30 μg/mL. Similarly, fractions 1−4 exhibited PXR activation at 30 μg/mL, inducing fold increases of 6.71, 2.75, 2.86, and 2.11, respectively (Figure 6A). Conversely, fractions 5−10 did not significantly

https://doi.org/10.1021/acsomega.4c08293
ACS Omega 2024, 9, 51394−51407

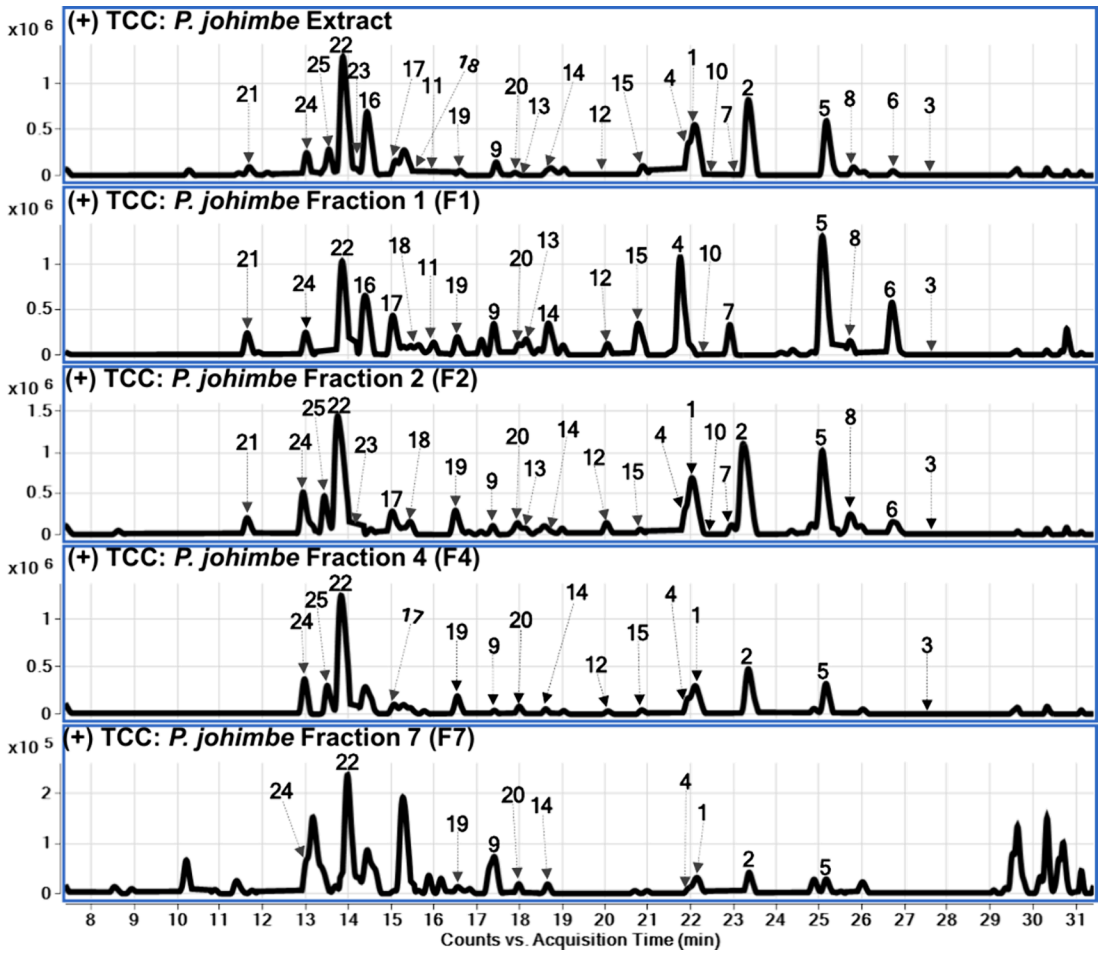

Figure 7. Total compound chromatograms of the *P. johimbe* extract along with corresponding fractions (F1, F2, F4, and F7) in positive ion mode.

activate PXR (Figure 6B), correlating with the absence of indole alkaloids. These findings suggest that the PXR-activating compounds (i.e., yohimbe alkaloids) reside in fractions 1−4.

Fraction 1 exhibited the strongest PXR activation, with a subsequent decrease in potency observed in fractions 2−4, indicating a concentration gradient of PXR activators. Subsequent analysis of pure alkaloids revealed that ajmalicine (**14**) significantly activated PXR, achieving a 3.21-fold increase at 30 μM. Additionally, yohimbine (**22**) and yohimbine *N*-oxide (**19**) demonstrated moderate PXR agonism (2.41- to 2.96-fold; Figure 6C). Hirsutine *N*-oxide (**27**), hirsuteine (**26**), and hirsuteine *N*-oxide (**28**) also exhibited moderate PXR induction (Figure 6C) but were not identified in *P. johimbe*. Among these, ajmalicine (**14**), yohimbine (**22**), and yohimbine *N*-oxide (**19**) exhibited optimal potency at 10 μM and a reduced activity at 30 μM. This suggests a potential for these compounds to interact with the PXR mechanism, potentially influencing its function and increasing the risk of HDIs, particularly in chronic disease states. Conversely, the remaining test compounds, ajmalicine *N*-oxide (**29**) and hirsutine (**3**) did not affect PXR activity (Figure 6D). Rifampicin, a drug clinically recognized for its PXR induction, was used as a positive control and showed a 3.65-fold increase in PXR activity at 10 μM (Figure 6E).

Since the inductive activity at PXR could now be attributed to a subset of the alkaloids present in *P. johimbe*, a bioassay-guided fractionation of the active *P. johimbe* extract revealed an enrichment of PXR inducers. As shown in Figure 6A, the fold activation of PXR decreased as the polarity of the mobile phase increased. The ethanolic extract had 4-fold induction (Figure 6) at 30 μM, while fraction 1 exhibited a 7-fold induction under identical concentration, indicating a 3-fold increase in activity due to the fractionation process and enrichment of certain alkaloids. PXR induction gradually decreased from 3-fold to 1-fold in fractions 2 through 10 (Figure 6A and Figure 6B). In cluster A (Figure 2 nodes with yellow label) corynantheine (**4**), corynantheidine (**1**), and its diastereomers (RT-22−26 min) were present in a higher abundance in fraction 1 (Figure 7); whereas, their abundance gradually decreased in fractions 2, 4, and 7 (Figure 7).

Ajmalicine (**14**), corynantheidine *N*-oxide (**6**), corynantheine *N*-oxide (**8**), and their epimers were present in higher abundance in fraction 1 (Figure 1: Clusters B, G, and H), suggesting that the aforementioned alkaloids may be responsible for the observed PXR induction.

***In Silico* Investigation of Yohimbe Alkaloid Agonism of PXR.** To corroborate the *in vitro* activation findings and to elucidate potential differential interactions among yohimbe alkaloids, molecular docking was employed to computationally characterize the binding conformations, energies, and receptor−ligand interaction profiles of yohimbine (**22**) and ajmalicine (**14**) at PXR. In recent years, *in silico* molecular docking has emerged as a prevalent tool for elucidating protein−ligand interactions, with successful applications in exploring the pharmacological potential of natural compounds at various biologically relevant targets.[36,37] Given the expansive ligand-binding domain of hPXR, induced fit docking (IFD) was

https://doi.org/10.1021/acsomega.4c08293
ACS Omega 2024, 9, 51394−51407

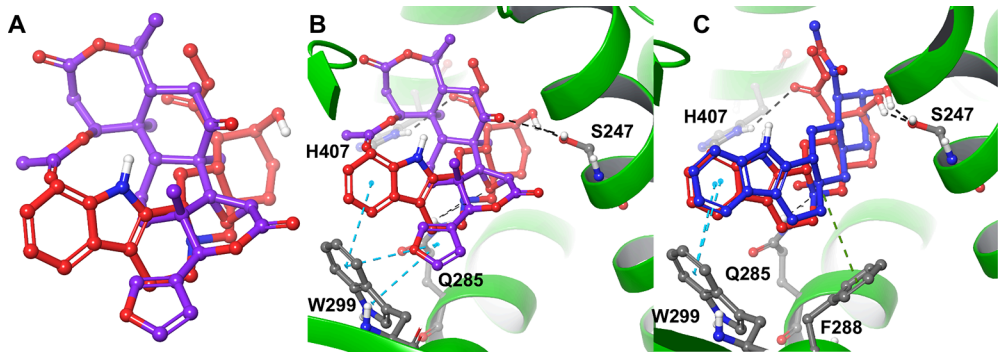

Figure 8. 3D visualization of IFD results for selected ligands within the PXR ligand-binding domain (LBD). (A) Most energetically favorable poses of nomilin (violet, ball-and-stick) and yohimbine (**22**) (red, ball-and-stick); (B) Interaction map between the LBD of PXR and both nomilin (violet, ball-and-stick) and yohimbine (**22**) (red, ball-and-stick); (C) Interactionmap between the LBD of PXR and yohimbine (**22**) (red, ball-and-stick) and (*S*)-yohimbine *N*-oxide (blue, ball-and-stick). Dashed lines represent H-bonding (black), π-cation (green), and $\pi-\pi$ stacking (cyan) interactions between the ligands and the receptor.

deemed an optimal methodology for modeling ligand binding, as it enables the prediction of ligand binding conformations in conjunction with concomitant structural adaptations within the receptor.[38]

Given the rigid, planar multicyclic core of yohimbe alkaloids, a crystal structure of hPXR complexed with a ligand structurally similar to indole alkaloids was sought from the Protein Data Bank (PDB) to serve as a suitable receptor model. This approach diverged from commonly used, more flexible synthetic and natural PXR agonists. A 2023 study by Fan et al.[39] identified nomilin, a citrus limonoid, as a PXR agonist with potency comparable to the established PXR activators, T0901317 and rifampicin.[39,40] The PXR−nomilin complex (PDB ID: 7YFK) was thus selected for subsequent IFD simulations with yohimbe alkaloids. The reliability of the docking protocol was validated through the redocking of nomilin. To comprehensively assess potential PXR interactions, both enantiomers of the *N*-oxide alkaloids were included in the docking study. IFD results demonstrated a strong correlation with the *in vitro* PXR activation data for yohimbine (**22**) and ajmalicine (**14**) along with their respective *N*-oxides (Figures 8 and 9 and Figures S37 and S38).

Comparative structural analysis revealed that nomilin and yohimbine occupied distinct regions within the PXR ligand-binding domain (Figure 8). Despite their different binding orientations, both nomilin and yohimbine (**22**) form critical interactions with four residues previously highlighted by Fan et al.[39] Notably for the yohimbine analogs, (*S*)-yohimbine *N*-oxide exhibited a unique π-cation interaction between its charged nitrogen and F288 of PXR (Figure 8C and Figure 9D). Comparative analysis of 2D interaction diagrams revealed that while yohimbine (**22**) formed H-bonds with three key polar residues as described by Fan et al. (Figure 9B), (*S*)-yohimbine *N*-oxide formed two H-bonds and a π-cation interaction at this site (Figure 9D).[39] Although yohimbine and its diastereomeric *N*-oxide analogs displayed $\pi-\pi$ stacking with W299, (*R*)-yohimbine *N*-oxide relied solely on $\pi-\pi$ interactions for binding to PXR (Figure 9C). Quantitative docking scores, including GlideScore, Glide Emodel, and Gibbs free energy values for each ligand−receptor complex are provided in Table 2.

CONCLUSIONS

In summary, molecular networking analysis of the ethanolic extract and fractions F1−F10 of *P. johimbe* enabled the expedited identification of yohimbe alkaloids. By applying MS/MS molecular networking, the identified alkaloids were classified into distinct clusters, revealing three oxindole alkaloids, 14 indole alkaloids, and eight *N*-oxide indole alkaloids based on structural similarities and mass spectral features. In addition, the ethanolic extract and its fractions were evaluated for PXR inductive activity. Yohimbine (**22**) and ajmalicine (**14**) were distinguished as the potential causative agents of PXR induction, compared to the activities of their counterparts. Molecular docking studies provided further insight and revealed that oxidation of yohimbe constituents to the corresponding *N*-4 oxides significantly alters the predicted interactions with the PXR ligand binding domain. Moreover, the presence of a methoxy acrylate moiety (an open form of E-ring) was tentatively postulated as a structural feature essential for PXR inductive potential among the identified yohimbe alkaloids.

EXPERIMENTAL SECTION

General Experimental Procedures. *Chemicals.* The reference standards, yohimbine (**22**), corynanthine (**21**), rauwolscine (**23**), ajmalicine (**14**), hirsutine (**3**), hirsuteine (**26**), and rifampicin were purchased from Sigma-Aldrich (St. Louis, MO, USA). The purity of reference standards was >98%. Acetonitrile, dichloromethane, methanol, ethanol, and formic acid (HPLC grade) were obtained from Fisher Scientific (Waltham, MA, USA). DMEM-F12, HEPES, trypsin EDTA, penicillin-streptomycin solution, and sodium pyruvate were purchased from GIBCO BRL, Invitrogen Corp. USA. FBS was purchased from Hyclone Lab Inc. (Utah, USA). Water was purified using a Millipore Milli-Q system (Bedford, MA, USA).

Plant Material. The dried bark of *P. johimbe* was purchased from a reputable botanical supplier. The rhizome material was authenticated morphologically and chemically by comparison with the botanical reference material at the National Center for Natural Products Research (NCNPR). The commercial bark sample (#1086) has been deposited as a reference at the NCNPR's botanical repository at the University of Mississippi (University, MS, USA).

Extraction and Isolation. The air-dried *P. johimbe* bark (14.56 g) was ground into a fine powder and extracted with 95% ethanol in an accelerated solvent extraction instrument for 45 min. The extract was concentrated under reduced pressure to yield a dark brown residue (1.79 g). A portion of this residue (528 mg) was subjected to flash chromatography using a 25 g

https://doi.org/10.1021/acsomega.4c08293
ACS Omega 2024, 9, 51394−51407

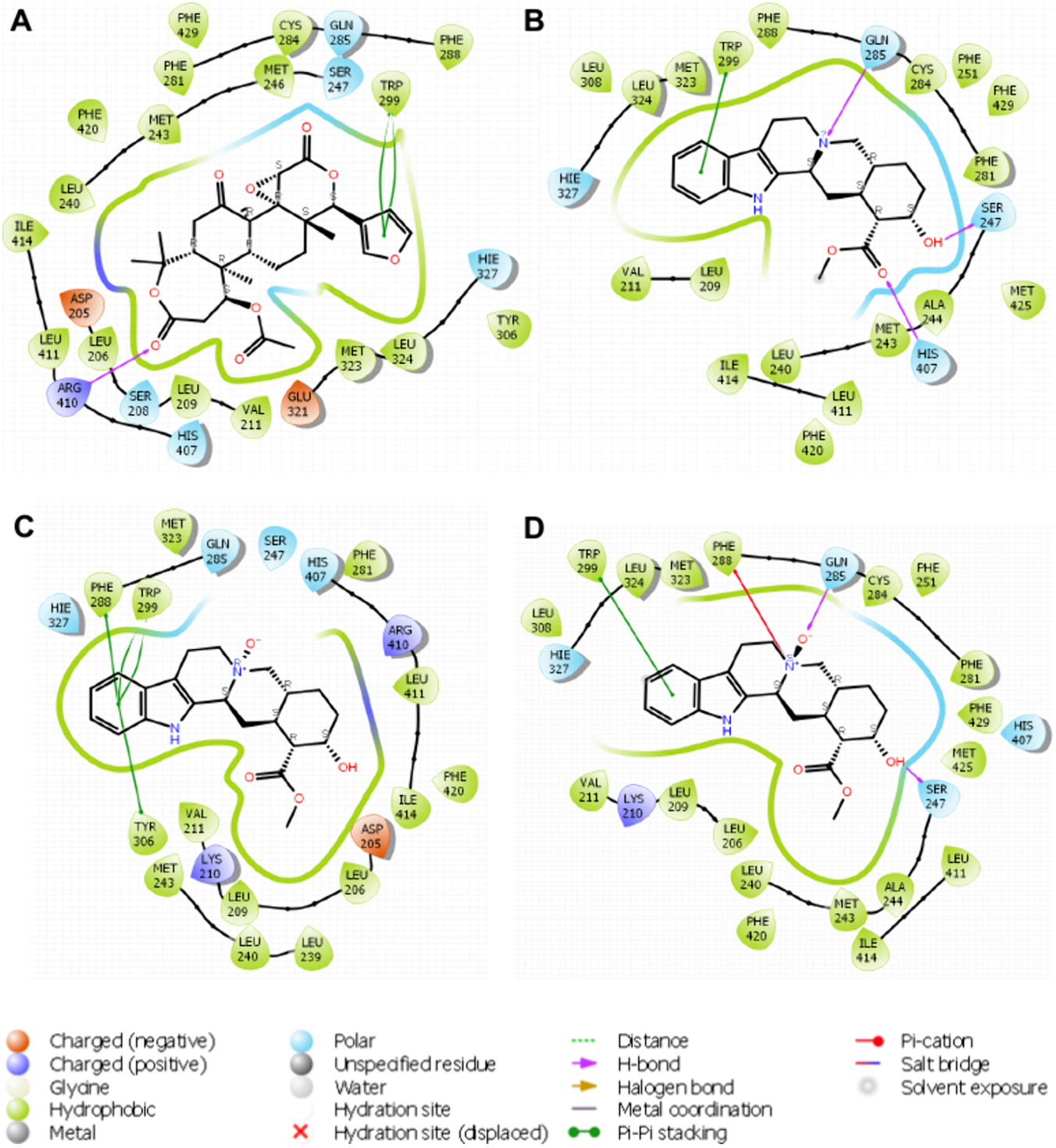

Figure 9. 2D interaction diagrams of selected ligands within the PXR binding site: (A) nomilin, (B) yohimbine (**22**), (C) (*R*)-yohimbine *N*-oxide, and (D) (*S*)-yohimbine *N*-oxide.

SNAP-KP-Si cartridge with a gradient of dichloromethane-methanol (100:0 to 0:100) at 20 mL/min to afford 10 fractions (F1−F10).

Preparation of Yohimbine N-Oxide.[19] To a stirred solution of yohimbine (25 mg, 70.53 μmol) in dry dichloromethane (1 mL), a solution of meta-chloroperbenzoic acid (19 mg, 85 μmol) in dry dichloromethane (1 mL) was added at −40 °C under argon atmosphere. After the reaction mixture was stirred for 4 h, the reaction mixture was poured into a chilled 5% $NaHCO_3$ solution and was extracted with chloroform. The combined organic layer was washed with brine, dried over Na_2SO_4, and evaporated. The residue was separated by SiO_2 column chromatography (20% methanol−chloroform) to give **19** (12 mg, 46%) as an amorphous powder. A similar route to yield all *N*-oxide alkaloids tested for PXR inductive activity is provided in Scheme S1.

^{1}H NMR (400 MHz, Methanol-d_4) δ 7.44 (d, J = 7.8 Hz, 1H), 7.33 (dd, J = 8.0, 0.9 Hz, 1H), 7.09 (t, J = 7.4 Hz, 1H), 7.02 (ddd,

https://doi.org/10.1021/acsomega.4c08293
ACS Omega 2024, 9, 51394−51407

Table 2. Calculated IFD Scores (Glide Score and Glide Emodel) and Binding Free Energies for PXR Ligands

Compound	Glide Score (kcal/mol)	Glide Emodel (kcal/mol)	Gibbs Free Energy (ΔG) (kcal/mol)
Nomilin (control)	−12.02	−97.82	−84.91
Yohimbine (**22**)	−12.08	−82.64	−70.54
(*R*)-Yohimbine *N*-oxide	−10.61	−65.26	−61.19
(*S*)-Yohimbine *N*-oxide	−12.61	−92.98	−73.15
Avg. Yohimbine *N*-oxide	−11.61	−79.12	−67.17
Ajmalicine (**14**)	−9.62	−79.60	−70.21
(*R*)-Ajmalicine *N*-oxide	−9.49	−79.28	−65.65
(*S*)-Ajmalicine *N*-oxide	−11.16	−84.94	−69.66
Avg. Ajmalicine *N*-oxide	−10.33	−82.11	−67.66

J = 8.0, 7.1, 1.1 Hz, 1H), 4.71 (brs, 1H), 4.29 (q, *J* = 2.8 Hz, 1H), 3.78 (s, 3H), 3.73−3.63 (m, 1H), 3.60−3.52 (m, 1H), 3.38 (s, 1H), 3.25 (s, 2H), 2.89 (d, *J* = 15.8 Hz, 1H), 2.52−2.45 (m, 1H), 2.45−2.37 (m, 1H), 2.30 (s, 1H), 2.14 (d, *J* = 11.1 Hz, 1H), 1.96 (dt, *J* = 13.7, 3.2 Hz, 1H), 1.85 (q, *J* = 12.4, 10.7 Hz, 1H), 1.72 (t, *J* = 13.6 Hz, 1H), 1.63−1.49 (m, 1H), 1.38 (d, *J* = 12.7 Hz, 1H).

LC-QToF-MS. The Agilent Series 1290 LC system (Santa Clara, CA, USA) used in analysis of the yohimbe samples was composed of the following modular components: a binary pump, a vacuum solvent microdegasser, an autosampler with 2 × 54-well tray, and a thermostatically controlled column compartment. Separation was achieved on an Agilent Poroshell C18 (2.1 × 150 mm, 2.7 μm) column. The mobile phase consisted of water with 0.1% formic acid (A) and acetonitrile with 0.1% formic acid (B) at a flow rate of 0.2 mL/min. Initial conditions consisted of a gradient elution of 10% B; 25 min, 33% B; 30 min, 100% B followed by column wash using 100% B in 5 min. One microliter of the sample was then injected. The column temperature was set to 40 °C. The MS analysis was performed with a QToF-MS/MS (Model #G6530A, Agilent Technologies, Santa Clara, CA, USA) equipped with an ESI source with Jet Stream technology using the following parameters: drying gas (N_2) flow rate, 13 L/min; drying gas temperature, 270 °C; nebulizer, 27 psi; sheath gas temperature, 300 °C; sheath gas flow, 11 L/min; capillary, 3500 V; skimmer, 60 V; Oct RF V, 750 V; and fragmentor voltage, 150 V. The acquisition was controlled by Agilent MassHunter Acquisition Software vA.05.01, and the data were processed with MassHunter Qualitative software vB.07.00. Standards were analyzed using targeted MS/MS where the quadrupole was set to an isolation width of 1.3 *m*/*z* for the precursor of each standard. MS/MS spectra were collected with collision offset voltages of 0, 10, 20, 30, and 40 V. Accurate mass measurements were obtained by means of reference ion correction using reference masses at *m*/*z* 121.0509 (protonated purine) and 922.0098 (protonated hexakis (1H, 1H, 3H-tetrafluoropropoxy) phosphazine or HP-921) in positive ion mode.

P. johimbe extract and fractions (concentration 2 mg/mL) were analyzed using an optimized data-dependent acquisition mode consisting of a full MS survey scan in the 100−1700 Da range (scan time:100 ms) followed by an MS/MS scan for the three most intense ions. The collision energy was applied over a gradient from 20 to 80 V.

Molecular Networking Analysis. The molecular network was created using the GNPS platform (https://gnps.ucsd.edu) with reliability enhanced by data preprocessing using MZmine 2.30 software.[41] Data were first converted to.mzML format with MSconvert. The .mzML files were imported into MZmine 2.30. Mass detection was achieved with noise levels of 1000 (MS) and 100 (MS/MS). The chromatograms were built from ions with a minimum time span of 0.01 min, a minimum height of 0, and a *m*/*z* tolerance of 0.001 (5.0 ppm). Chromatographic deconvolution was performed by a baseline cutoff algorithm with the following parameters: minimum peak height of 200, peak duration range of 0 to 10 min, and baseline level of 50. Chromatograms were deisotoped using the isotopic peaks grouper algorithm with an *m*/*z* tolerance of 0.001 (5.0 ppm) and retention time tolerance of 0.1 min. A duplicated peak filter was applied with a *m*/*z* tolerance of 0.001 (or 5.0 ppm) and RT tolerance of 0.1 min. Join alignment was performed with a *m*/*z* tolerance 0.001 (5.0 ppm). A peak row filter was applied with a *m*/*z* to all processed peak list within the *m*/*z* 300−400 range. Only peaks with the MS2 scan (GNPS) were retained, and the peak number IDs were reset. Finally, the aligned peak list was exported as a.mgf file for GNPS from which spectral data were uploaded to the GNPS molecular networking platform (https://gnps.ucsd.edu).[42] A network was then created where edges were filtered to have a cosine score of >0.7 and more than six matched peaks. Edges between two nodes were kept in the network if each node appeared in the other's respective top 10 most similar nodes. The spectra in the network were then searched against the GNPS spectral libraries. All matches kept between network spectra and library spectra were required to be above 0.7 and maintain at least four matched peaks. The output was visualized using Cytoscape 3.7.1 software.[43] The GNPS job parameters and resulting data are available at the following address: (https://gnps.ucsd.edu/ProteoSAFe/status.jsp?task=20c7d155f6404fd89159445b04bfb34e).

Cell Culture and Treatment. Human hepatocellular carcinoma cell line (HepG2) was obtained from the American Type Culture Collection (ATCC) and maintained and cultured in DMEM/F12 medium supplemented with 10% FBS, 2.4 g/L sodium bicarbonate, 100 μg/mL streptomycin, and 100 units/mL penicillin. Cells were grown at 37 °C in a 5% CO_2 environment with 98% relative humidity. The stocks of extract (20 mg/mL), pure phytochemicals (10 mM), and positive control (10 mM) were prepared in DMSO and stored at 4 °C in a refrigerator.

Reporter Gene Assay for PXR Activation. For examination of PXR activation, HepG2 cells were transfected with pSG5-hPXR (25 μg), and PCR-5 (25 μg) plasmid by electroporation at 180 V (1 pulse for 70 m sec). Cells were incubated for 8 min at room temperature in a biosafety cabinet and floating dead cells were removed. The remaining cells were suspended in DMEM/F12 medium and seeded in 96-well plates at a density of 50,000 cells per well. After reaching 70 to 90% confluency, cells were incubated with increasing concentrations of extract, fractions (0.12, 0.37 1.13, 3.33, 10, and 30 μg/mL), pure phytochemicals (0.12, 0.37 1.13, 3.33, 10, and 30, μM), and positive control (rifampicin; 0.6, 0.12, 0.37, 1.11, 3.33, and 10 μM) for 24 h. Next, the culture medium was aspirated, and 40 μL luciferase reagent (Promega Corporation, USA) was added to each well. Luminescence was measured using a SpectraMax M5 fluorescence plate reader (Molecular Devices, USA), and the fold increase in luciferase activity among sample-treated cells

https://doi.org/10.1021/acsomega.4c08293
ACS Omega 2024, 9, 51394−51407

was calculated compared with the vehicle-treated (DMSO) cells.[44]

***In Silico* Molecular Docking.** *Ligands and Receptor Preparation.* The recently released X-ray structure of PXR cocrystallized with the specific agonist nomilin (PDB ID: 7YFK) was retrieved from PDB.[39] The Schrödinger Maestro platform (version 12.8) with its integrated Protein Preparation Wizard was used to process the PXR protein structure.[45,46] This involved optimization and refinement for molecular docking. The protein receptor was preprocessed at a pH of 7.4 ± 2.0, and missing side chains and loops were filled in with Prime.[47−49] H-bonds were also assigned at a pH of 7.4. Additionally, all ligands to be docked were conformationally optimized with the LigPrep module, again at a pH of 7.4 ± 2.0.[50] In both the protein and ligand preparation steps, the OPLS4 force field was applied.[51]

Induced Fit Molecular Docking. Since the IFD protocol developed by Schrödinger simultaneously incorporates Glide and Prime to predict conformational changes of both the ligands and the receptor upon binding, it can accurately model active sites of complex receptors such as PXR (www.schrodinger.com).[52−55] The standard protocol to generate up to 20 poses was selected for the IFD method. Using the published position of nomilin bound to PXR, the receptor box center was positioned on the centroid of nomilin in the structure from PDB ID: 7YFK.[39] No constraints were placed on the docking method. The conformational sampling of the protocol was set to dock the ligands rigidly and sample ring conformations within a window of 2.5 kcal/mol. Additionally, the side chains of the receptor were trimmed and optimized. Finally, the Glide method allowed for redocking into structures within 15.0 kcal/mol of the best structure and within the top 20 structures overall at extra precision.[56−60] Previous redocking protocols have been demonstrated to produce similar crystallographic poses of ligands from other PXR crystal structures.[61]

The best poses of each ligand were selected based on GlideScores and Glide Emodels for the ligand−receptor complexes. The Glide Emodel score was used to select the most favorable pose among multiple poses for each ligand. Following prioritization of the optimal poses for the yohimbe alkaloids, Prime MM-GBSA calculations were carried out with the OPLS4 force field in the VSGB solvation model.[49,51]

■ ASSOCIATED CONTENT

Supporting Information

The Supporting Information is available free of charge at https://pubs.acs.org/doi/10.1021/acsomega.4c08293.

Synthetic route for *N*-oxide alkaloid preparation, MS/MS spectra and proposed fragmentation pathways of compounds **1**−**25**, and additional IFD docking results (PDF)

■ AUTHOR INFORMATION

Corresponding Author

Amar G. Chittiboyina − *National Center for Natural Products Research, School of Pharmacy, University of Mississippi, University, Mississippi 38677-1848, United States;* orcid.org/0000-0002-7047-5373; Phone: 1-662-915-1572; Email: amar@olemiss.edu; Fax: 1-662-915-7989

Authors

Suresh Chandra V. A. R. Annam − *National Center for Natural Products Research, School of Pharmacy, University of Mississippi, University, Mississippi 38677-1848, United States*

William M. Neal − *National Center for Natural Products Research, School of Pharmacy, University of Mississippi, University, Mississippi 38677-1848, United States*

Pankaj Pandey − *National Center for Natural Products Research, School of Pharmacy, University of Mississippi, University, Mississippi 38677-1848, United States;* orcid.org/0000-0001-9128-8254

Bharathi Avula − *National Center for Natural Products Research, School of Pharmacy, University of Mississippi, University, Mississippi 38677-1848, United States*

Kumar Katragunta − *National Center for Natural Products Research, School of Pharmacy, University of Mississippi, University, Mississippi 38677-1848, United States;* orcid.org/0000-0002-8787-4602

Islam Husain − *National Center for Natural Products Research, School of Pharmacy, University of Mississippi, University, Mississippi 38677-1848, United States*

Shabana I. Khan − *National Center for Natural Products Research, School of Pharmacy and Department of BioMolecular Sciences, Division of Pharmacognosy, School of Pharmacy, University of Mississippi, University, Mississippi 38677-1848, United States;* orcid.org/0000-0001-6429-7219

Igor Koturbash − *Department of Environmental Health Sciences, University of Arkansas for Medical Sciences, Little Rock, Arkansas 72205-7199, United States*

Bill J. Gurley − *National Center for Natural Products Research, School of Pharmacy, University of Mississippi, University, Mississippi 38677-1848, United States*

Ikhlas A. Khan − *National Center for Natural Products Research, School of Pharmacy and Department of BioMolecular Sciences, Division of Pharmacognosy, School of Pharmacy, University of Mississippi, University, Mississippi 38677-1848, United States*

Complete contact information is available at: https://pubs.acs.org/10.1021/acsomega.4c08293

Notes

The authors declare no competing financial interest.

■ ACKNOWLEDGMENTS

This research is supported in part by "In vitro screening of a unique botanical extract collection for herb-drug interaction (HDI) potential" funded by the National Center for Complementary & Integrative Health, NIH grant number 5R21AT011107, and "Science-Based Authentication of Botanical Ingredients" funded by the Center for Food Safety and Applied Nutrition, US FDA grant number 5U01FD004246.

■ REFERENCES

(1) Dias, D. A.; Urban, S.; Roessner, U. A historical overview of natural products in drug discovery. *Metabolites* **2012**, *2* (2), 303−336.

(2) Wu, C.; Lee, S.-L.; Taylor, C.; Li, J.; Chan, Y.-M.; Agarwal, R.; Temple, R.; Throckmorton, D.; Tyner, K. Scientific and regulatory approach to botanical drug development: a US FDA perspective. *J. Nat. Prod.* **2020**, *83* (2), 552−562.

(3) Kellogg, J. J.; Paine, M. F.; McCune, J. S.; Oberlies, N. H.; Cech, N. B. Selection and characterization of botanical natural products for

research studies: a NaPDI center recommended approach. *Nat. Prod. Rep.* **2019**, *36* (8), 1196−1221.
(4) van Breemen, R. B. Development of Safe and Effective Botanical Dietary Supplements: Miniperspective. *J. Med. Chem.* **2015**, *58* (21), 8360−8372.
(5) Hukkanen, J.; Hakkola, J.; Rysä, J. Pregnane X receptor (PXR)−a contributor to the diabetes epidemic? *Drug Metabol. Drug Interact.* **2014**, *29* (1), 3−15.
(6) Additives, E. P. O. F.; Food, N. S. A. T. Scientific Opinion on the evaluation of the safety in use of Yohimbe (Pausinystalia yohimbe (K. Schum.) Pierre ex Beille). *EFSA Journal* **2013**, *11* (7), 3302.
(7) Ho, C.-T.. *African Natural Plant Products: New Discoveries and Challenges In Chemistry and Quality. OUP Catalogue*;Juliani, H. R., Simon, J., Eds.; Oxford University Press: 2010; number 9780841269873.
(8) Clark, L. E.; Sunderland, T. C. *The key non-timber forest products of Central Africa: state of the knowledge*; U.S. Agency for International Development (USAID): 2004.
(9) Orwa, C.http://www.worldagroforestry.org/sites/treedbs/treedatabases. asp **2009**.
(10) Wenkert, E.; Bindra, J. S.; Chang, C.-J.; Cochran, D. W.; Schell, F. M. Carbon-13 nuclear magnetic resonance spectroscopy of naturally occurring substances. *Alkaloids Acc. Chem. Res.* **1974**, *7* (2), 46−51.
(11) Simms, J. A.; Richards, J. K.; Mill, D.; Kanholm, I.; Holgate, J. Y.; Bartlett, S. E. Induction of multiple reinstatements of ethanol-and sucrose-seeking behavior in Long−Evans rats by the α-2 adrenoreceptor antagonist yohimbine. *J. Psychopharmacol.* **2011**, *218*, 101−110.
(12) Mills, S.; Bone, K. *Principles and practice of phytotherapy*; Churchill Livingstone: Oxford, 2000.
(13) Jabir, N. R.; Firoz, C. K.; Zughaibi, T. A.; Alsaadi, M. A.; Abuzenadah, A. M.; Al-Asmari, A. I.; Alsaieedi, A.; Ahmed, B. A.; Ramu, A. K.; Tabrez, S. A literature perspective on the pharmacological applications of yohimbine. *Ann. Med.* **2022**, *54* (1), 2849−2863.
(14) Millan, M. J.; Newman-Tancredi, A.; Audinot, V.; Cussac, D.; Lejeune, F.; Nicolas, J. P.; Cogé, F.; Galizzi, J. P.; Boutin, J. A.; Rivet, J. M. Agonist and antagonist actions of yohimbine as compared to fluparoxan at α2-adrenergic receptors (AR) s, serotonin (5-HT) 1A, 5-HT1B, 5-HT1D and dopamine D2 and D3 receptors. Significance for the modulation of frontocortical monoaminergic transmission and depressive states. *Synapse* **2000**, *35* (2), 79−95.
(15) Haller, C. A.; Kearney, T.; Bent, S.; Ko, R.; Benowitz, N. L.; Olson, K. Dietary supplement adverse events: report of a one-year poison center surveillance project. *J. Med. Toxicol.* **2008**, *4*, 84−92.
(16) Estes, J. d. High prevalence of potentially hepatotoxic herbal supplement use in patients with fulminant hepatic failure. *Arch Surg.* **2003**, *138* (8), 852−858.
(17) Favreau, J. T.; Ryu, M. L.; Braunstein, G.; Orshansky, G.; Park, S. S.; Coody, G. L.; Love, L. A.; Fong, T.-L. Severe hepatotoxicity associated with the dietary supplement LipoKinetix. *Ann. Int. Med.* **2002**, *136* (8), 590−595.
(18) Miousse, I. R.; Skinner, C. M.; Lin, H.; Ewing, L. E.; Kosanke, S. D.; Williams, D. K.; Avula, B.; Khan, I. A.; ElSohly, M. A.; Gurley, B. J.; Koturbash, I. Safety assessment of the dietary supplement OxyELITE Pro (New Formula) in inbred and outbred mouse strains. *Food Chem. Toxicol.* **2017**, *109*, 194−209.
(19) Zhan, G.; Miao, R.; Zhang, F.; Wang, X.; Zhang, X.; Guo, Z. Cytotoxic yohimbine-type alkaloids from the leaves of Rauvolfia vomitoria. *Chem. Biodivers.* **2020**, *17* (12), No. e2000647.
(20) Phaya, M.; Chalom, S.; Ingkaninan, K.; Ounnunkad, K.; Chandet, N.; Pyne, S. G.; Mungkornasawakul, P. Oxidative biotransformation of stemofoline alkaloids. *Artif. Cells Nanomed. Biotechnol.* **2021**, *49* (1), 166−172.
(21) Damani, L. A.; Pool, W. F.; Crooks, P. A.; Kaderlik, R. K.; Ziegler, D. M. Stereoselectivity in the N'-oxidation of nicotine isomers by flavin-containing monooxygenase. *Mol. Pharmacol.* **1988**, *33* (6), 702−705.
(22) Liu, Y.; Yu, H.-Y.; Xu, H.-Z.; Liu, J.-J.; Meng, X.-G.; Zhou, M.; Ruan, H.-L. Alkaloids with Immunosuppressive Activity from the Bark of Pausinystalia yohimbe. *J. Nat. Prod.* **2018**, *81* (8), 1841−1849.
(23) Ehmke, A.; von Borstel, K.; Hartmann, T. Alkaloid N-oxides as transport and vacuolar storage compounds of pyrrolizidine alkaloids in Senecio vulgaris L. *Planta* **1988**, *176*, 83−90.
(24) Butterweck, V.; Nahrstedt, A.; Evans, J.; Hufeisen, S.; Rauser, L.; Savage, J.; Popadak, B.; Ernsberger, P.; Roth, B. L. In vitro receptor screening of pure constituents of St. John's wort reveals novel interactions with a number of GPCRs. *J. Psychopharmacol.* **2002**, *162*, 193−202.
(25) Watkins, R. E.; Maglich, J. M.; Moore, L. B.; Wisely, G. B.; Noble, S. M.; Davis-Searles, P. R.; Lambert, M. H.; Kliewer, S. A.; Redinbo, M. R. 2.1 Å crystal structure of human PXR in complex with the St. John's wort compound hyperforin. *Biochem.* **2003**, *42* (6), 1430−1438.
(26) Mangelsdorf, D. J.; Thummel, C.; Beato, M.; Herrlich, P.; Schutz, G.; Umesono, K.; Blumberg, B.; Kastner, P.; Mark, M.; Chambon, P.; Evans, R. M. The nuclear receptor superfamily: the second decade. *Cell* **1995**, *83* (6), 835−839.
(27) Sever, R.; Glass, C. K. Signaling by nuclear receptors. *Cold Spring Harb. Perspect. Biol.* **2013**, *5* (3), No. a016709.
(28) Niu, X.; Wu, T.; Li, G.; Gu, X.; Tian, Y.; Cui, H. Insights into the critical role of the PXR in preventing carcinogenesis and chemotherapeutic drug resistance. *Int. J. Biol. Sci.* **2022**, *18* (2), 742.
(29) Watkins, R. E.; Wisely, G. B.; Moore, L. B.; Collins, J. L.; Lambert, M. H.; Williams, S. P.; Willson, T. M.; Kliewer, S. A.; Redinbo, M. R. The human nuclear xenobiotic receptor PXR: structural determinants of directed promiscuity. *Science* **2001**, *292* (5525), 2329−2333.
(30) Mani, S.; Dou, W.; Redinbo, M. R. PXR antagonists and implication in drug metabolism. *Drug Metab. Rev.* **2013**, *45* (1), 60−72.
(31) Oladimeji, P. O.; Chen, T. PXR: more than just a master xenobiotic receptor. *Mol. Pharmacol.* **2018**, *93* (2), 119−127.
(32) Wang, M.; Carver, J. J.; Phelan, V. V.; Sanchez, L. M.; Garg, N.; Peng, Y.; Nguyen, D. D.; Watrous, J.; Kapono, C. A.; Luzzatto-Knaan, T. Sharing and community curation of mass spectrometry data with Global Natural Products Social Molecular Networking. *Nat. Biotechnol.* **2016**, *34* (8), 828−837.
(33) Kumar, S.; Singh, A.; Bajpai, V.; Srivastava, M.; Singh, B. P.; Kumar, B. Structural characterization of monoterpene indole alkaloids in ethanolic extracts of Rauwolfia species by liquid chromatography with quadrupole time-of-flight mass spectrometry. *J. Pharm. Anal* **2016**, *6* (6), 363−373.
(34) Wang, H.-B.; Qi, W.; Zhang, L.; Yuan, D. Qualitative and quantitative analyses of alkaloids in Uncaria species by UPLC-ESI-Q-TOF/MS. *Chem. Pharm. Bull.* **2014**, *62* (11), 1100−1109.
(35) Sun, J.; Baker, A.; Chen, P. Profiling the indole alkaloids in yohimbe bark with ultra-performance liquid chromatography coupled with ion mobility quadrupole time-of-flight mass spectrometry. *Rapid Commun. Mass Spectrom.* **2011**, *25* (18), 2591−2602.
(36) Saini, N.; Grewal, A. S.; Lather, V.; Gahlawat, S. K. Natural alkaloids targeting EGFR in non-small cell lung cancer: Molecular docking and ADMET predictions. *Chemico-Biological Interactions* **2022**, *358*, No. 109901.
(37) Shah, M.; Yamin, R.; Ahmad, I.; Wu, G.; Jahangir, Z.; Shamim, A.; Nawaz, H.; Nishan, U.; Ullah, R.; Ali, E. A. In-silico evaluation of natural alkaloids against the main protease and spike glycoprotein as potential therapeutic agents for SARS-CoV-2. *PLoS One* **2024**, *19* (1), No. e0294769.
(38) Sherman, W.; Day, T.; Jacobson, M. P.; Friesner, R. A.; Farid, R. Novel procedure for modeling ligand/receptor induced fit effects. *J. Med. Chem.* **2006**, *49* (2), 534−553.
(39) Fan, S.; Yan, Y.; Xia, Y.; Zhou, Z.; Luo, L.; Zhu, M.; Han, Y.; Yao, D.; Zhang, L.; Fang, M. Pregnane X receptor agonist nomilin extends lifespan and healthspan in preclinical models through detoxification functions. *Nat. Commun.* **2023**, *14* (1), 3368.
(40) Seow, C. L.; Lau, A. J. Differential activation of pregnane X receptor by carnosic acid, carnosol, ursolic acid, and rosmarinic acid. *Pharmacol. Res.* **2017**, *120*, 23−33.
(41) Pluskal, T.; Castillo, S.; Villar-Briones, A.; Orešič, M. MZmine 2: modular framework for processing, visualizing, and analyzing mass

https://doi.org/10.1021/acsomega.4c08293
ACS Omega 2024, 9, 51394−51407

spectrometry-based molecular profile data. *BMC bioinformatics* **2010**, *11*, 1−11.
(42) Wang, M.; Carver, J. J.; Phelan, V. V.; Sanchez, L. M.; Garg, N.; Peng, Y.; Nguyen, D. D.; Watrous, J.; Kapono, C. A.; Luzzatto-Knaan, T. Sharing and community curation of mass spectrometry data with Global Natural Products Social Molecular Networking. *Nat. Biotechnol.* **2016**, *34* (8), 828−837.
(43) Gustavsen, J. A.; Pai, S.; Isserlin, R.; Demchak, B.; Pico, A. R. *F1000Research* **2019**, *8*, 1774.
(44) Husain, I.; Dale, O. R.; Martin, K.; Gurley, B. J.; Adams, S. J.; Avula, B.; Chittiboyina, A. G.; Khan, I. A.; Khan, S. I. Screening of medicinal plants for possible herb-drug interactions through modulating nuclear receptors, drug-metabolizing enzymes and transporters. *J. Ethnopharmacol.* **2023**, *301*, No. 115822.
(45) Madhavi Sastry, G.; Adzhigirey, M.; Day, T.; Annabhimoju, R.; Sherman, W. Protein and ligand preparation: parameters, protocols, and influence on virtual screening enrichments. *J. Comput. Aided Mol. Des.* **2013**, *27*, 221−234.
(46) *Schrödinger Release 2021−2: Protein Preparation Wizard*; Epik, Schrödinger, LLC, New York, NY, 2021; Impact, Schrödinger, LLC, New York, NY; Prime, Schrödinger, LLC, New York, NY, 2021.
(47) Jacobson, M. P.; Pincus, D. L.; Rapp, C. S.; Day, T. J.; Honig, B.; Shaw, D. E.; Friesner, R. A. Proteins: Struct. *Funct., Bioinf.* **2004**, *55* (2), 351−367.
(48) Jacobson, M. P.; Friesner, R. A.; Xiang, Z.; Honig, B. On the role of the crystal environment in determining protein side-chain conformations. *J. Mol. Biol.* **2002**, *320* (3), 597−608.
(49) *Schrödinger Release 2021−2: Prime*; Schrödinger, LLC: New York, NY, 2021.
(50) *Schrödinger Release 2021−2: LigPrep*; Schrödinger, LLC: New York, NY, 2021.
(51) Lu, C.; Wu, C.; Ghoreishi, D.; Chen, W.; Wang, L.; Damm, W.; Ross, G. A.; Dahlgren, M. K.; Russell, E.; Von Bargen, C. D. OPLS4: Improving force field accuracy on challenging regimes of chemical space. *J. Chem. Theory Comput.* **2021**, *17* (7), 4291−4300.
(52) Farid, R.; Day, T.; Friesner, R. A.; Pearlstein, R. A. New insights about HERG blockade obtained from protein modeling, potential energy mapping, and docking studies. *Bioorg. Med. Chem. Lett.* **2006**, *14* (9), 3160−3173.
(53) Sherman, W.; Day, T.; Jacobson, M. P.; Friesner, R. A.; Farid, R. Novel procedure for modeling ligand/receptor induced fit effects. *J. Med. Chem.* **2006**, *49* (2), 534−553.
(54) Sherman, W.; Beard, H. S.; Farid, R. Use of an induced fit receptor structure in virtual screening. *Chem. Biol. Drug Des.* **2006**, *67* (1), 83−84.
(55) *Schrödinger Release 2021−2: Induced Fit Docking protocol*; Glide, Schrödinger, LLC, New York, NY, 2021; Prime, Schrödinger, LLC: New York, NY, 2021.
(56) Yang, Y.; Yao, K.; Repasky, M. P.; Leswing, K.; Abel, R.; Shoichet, B. K.; Jerome, S. V. Efficient exploration of chemical space with docking and deep learning. *J. Chem. Theory Comput.* **2021**, *17* (11), 7106−7119.
(57) Friesner, R. A.; Murphy, R. B.; Repasky, M. P.; Frye, L. L.; Greenwood, J. R.; Halgren, T. A.; Sanschagrin, P. C.; Mainz, D. T. Extra precision glide: Docking and scoring incorporating a model of hydrophobic enclosure for protein− ligand complexes. *J. Med. Chem.* **2006**, *49* (21), 6177−6196.
(58) Halgren, T. A.; Murphy, R. B.; Friesner, R. A.; Beard, H. S.; Frye, L. L.; Pollard, W. T.; Banks, J. L. Glide: a new approach for rapid, accurate docking and scoring. 2. Enrichment factors in database screening. *J. Med. Chem.* **2004**, *47* (7), 1750−1759.
(59) Friesner, R. A.; Banks, J. L.; Murphy, R. B.; Halgren, T. A.; Klicic, J. J.; Mainz, D. T.; Repasky, M. P.; Knoll, E. H.; Shelley, M.; Perry, J. K. Glide: a new approach for rapid, accurate docking and scoring. 1. Method and assessment of docking accuracy. *J. Med. Chem.* **2004**, *47* (7), 1739−1749.
(60) *Schrödinger Release 2021−2: Glide*; Schrödinger, LLC, New York, NY, 2021.
(61) Pandey, P.; Idrisi, M.; Ali, Z.; Husain, I.; Neal, W. M.; Khan, S. I.; Ferreira, D.; Chittiboyina, A. G.; Khan, I. A. iso-Guttiferone J and Structure Revision of Guttiferone J from Garcinia gummi-gutta: A Combined Experimental and Integrated QM/NMR Approach. *Planta Med.* **2024**, *90* (07/08), 631−640.

https://doi.org/10.1021/acsomega.4c08293
ACS Omega 2024, 9, 51394−51407